

## **Supporting Information**

### **Fabrication of An Inexpensive Hydrophilic Bridge on A Carbon Substrate and Loading Vanadium Sulfides for Flexible Aqueous Zinc-ion Batteries**

Sainan Liu<sup>a,b</sup>, Xinxiang Chen<sup>c</sup>, Qiang Zhang<sup>a,b</sup>, Jiang Zhou<sup>c</sup>, Zhenyang Cai<sup>c\*</sup>, Anqiang Pan<sup>c\*</sup>

<sup>a</sup> *School of Minerals Processing and Bioengineering, Central South University, Changsha 410083, China.*

<sup>b</sup> *Hunan Key Lab of Mineral Materials and Application, Central South University, Changsha 410083, China.*

<sup>c</sup> *School of Materials Science and Engineering, Central South University, Changsha 410083, China*

\*Corresponding author, Email: csuczy@csu.edu.cn, pananqiang@csu.edu.cn

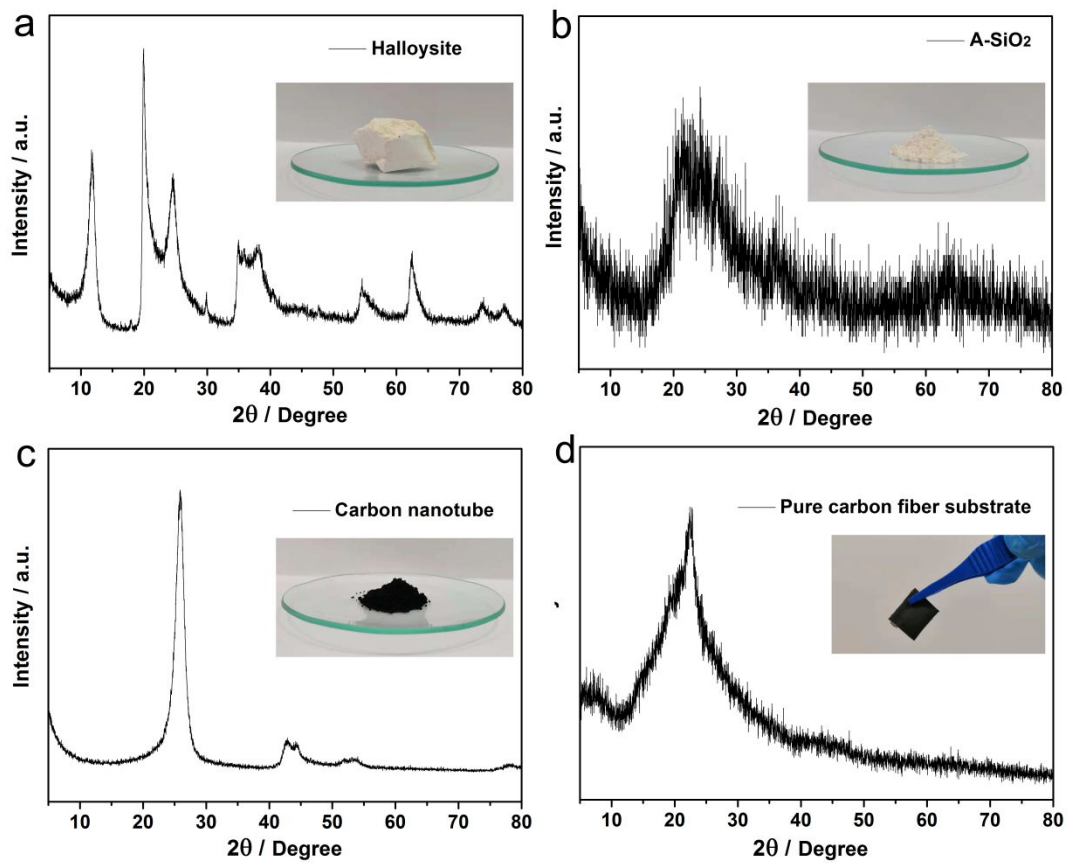


**Figure S1** XRD patterns of (a) natural halloysite, (b) A-SiO<sub>2</sub>, (c) commercial carbon nanotubes, and (d) pure carbon fiber substrate. Insets: macroscopic photographs of each sample.

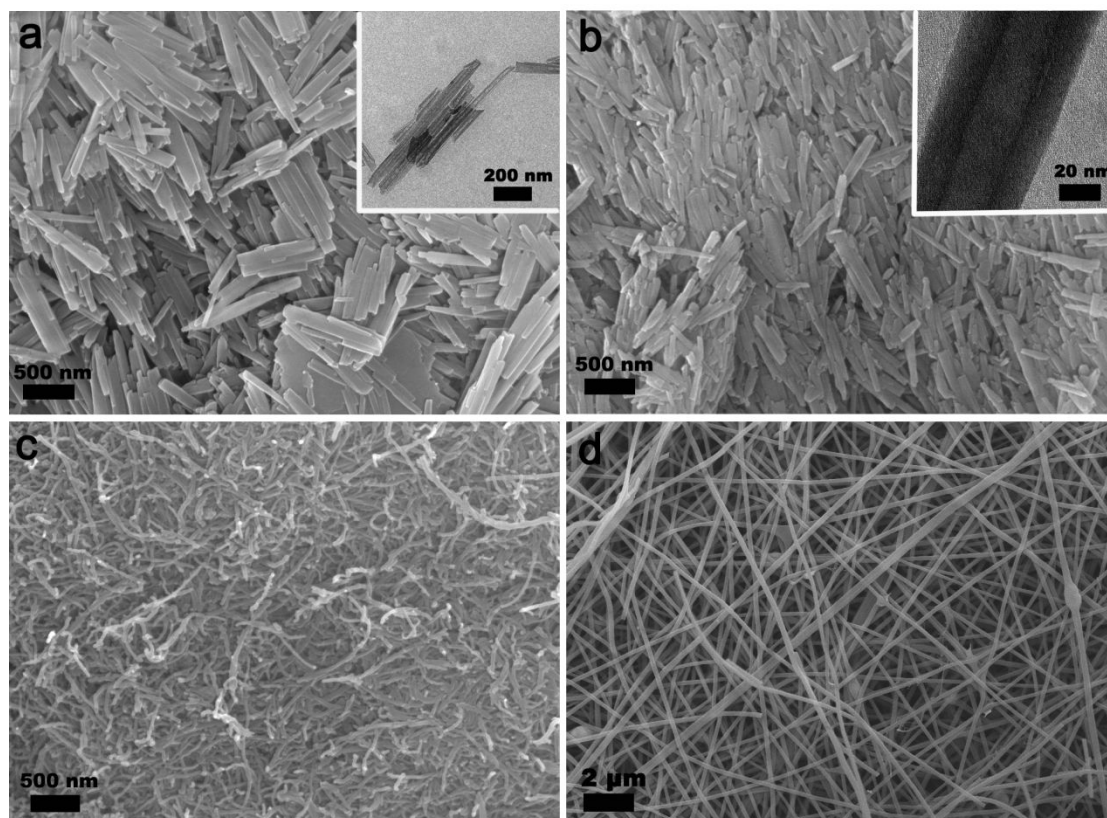


**Figure S2** Microscale morphology of samples. (a) SEM image and TEM image (inset) of natural halloysite; (b) SEM image and TEM image (inset) of A-SiO<sub>2</sub>; (c) SEM image of commercial carbon nanotubes; and (d) SEM image of the pure carbon fiber substrate.

The original halloysite clay morphology exhibits nanotubes with lengths of 0.8–1.0 μm, an average external diameter of 80–100 nm, and an average lumen diameter of 20–40 nm. After selective acid etching, the obtained A-SiO<sub>2</sub> retains its original tubular morphology, but with a shorter length of 0.2–0.5 μm. The commercial carbon nanotubes exhibit a curved tubular morphology, and the pure carbon substrate fiber exhibits a smooth surface.

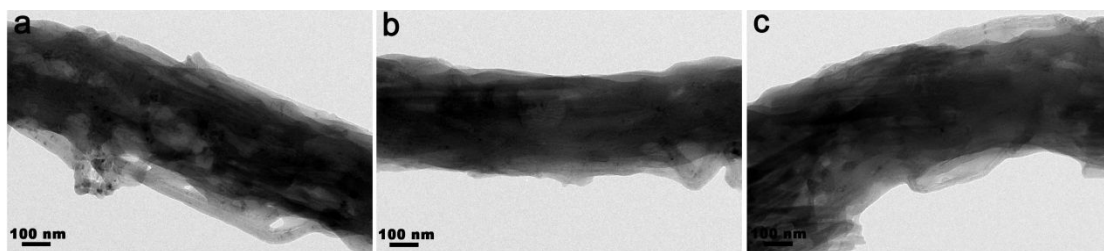


**Figure S3** Some representative TEM images of the HCC substrate, showing that A-SiO<sub>2</sub> and carbon nanotubes are uniformly composited on the surface of carbon fibers.

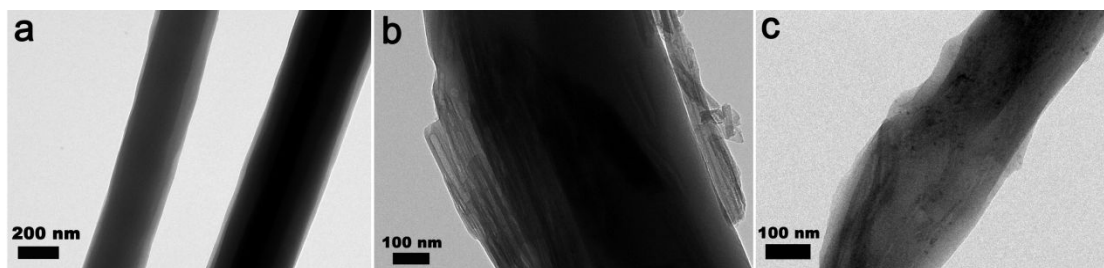


**Figure S4** TEM images of (a) pure carbon fiber substrate, (b) HC, and (c) CC substrate.

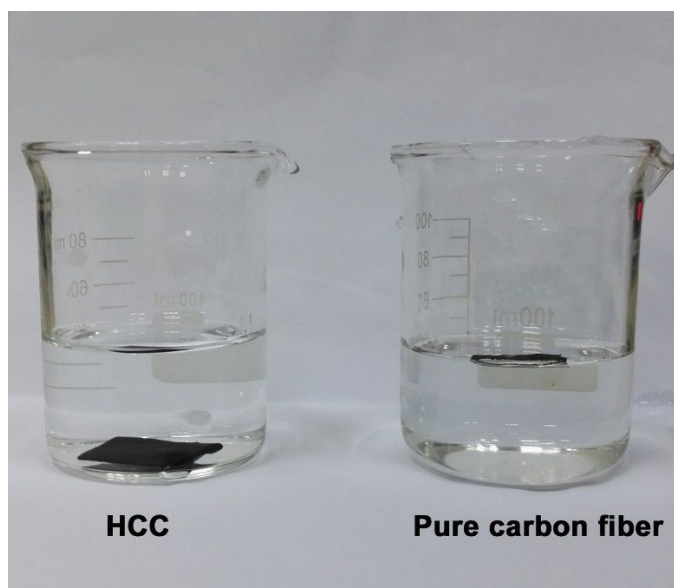


**Figure S5** Macroscopic digital photos of the intuitive hydrophilicity test of HCC and pure carbon fiber substrates.

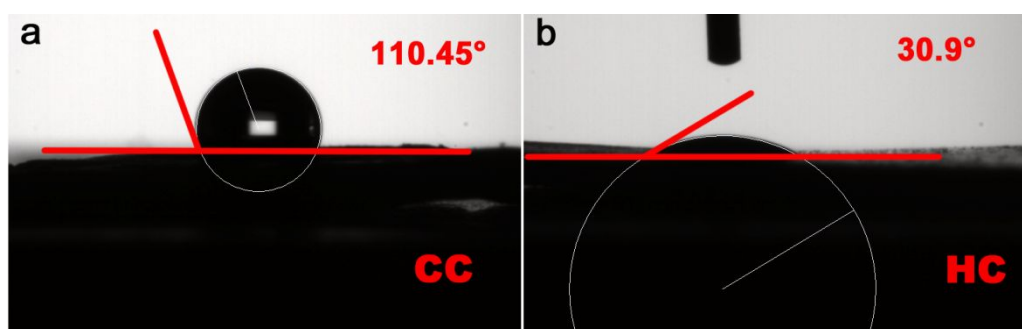


**Figure S6** Contact angles (CAs) of the (a) CC substrate and (b) pure carbon fiber substrate.

**Table S1** Observed vibration positions and their assignments from the FTIR spectra of different samples.

Position / $\text{cm}^{-1}$	Assignments
3690	Inner-surface -OH stretching vibrations of halloysite aluminol groups
3620	Inner -OH stretching vibrations of halloysite aluminol groups
a broad peak at 3200–3700 with a maximum at 3450	SiO–H vibrations
1643	-O–H deformation of water
a broad peak at 850–1300 with a maximum at 1040	in-plane Si–O–Si deformations
910	-O–H deformation of inner hydroxyls
790	Symmetric stretching of Si–O
750	Si–O–Al perpendicular stretching

### Method for Calculating the Physical Adsorption Energy.

First-principles calculations were performed with the density functional theory (DFT) using the Vienna Ab-initio Simulation Package (VASP) package. The generalized gradient approximation (GGA) with the Perdew–Burke–Ernzerhof (PBE) functional were used to describe the electronic exchange and correlation effects. Uniform G-centered k-points meshes with a resolution of  $2\pi \cdot 0.03 \text{ \AA}^{-1}$  and Methfessel–Paxton electronic smearing were adopted to integrate the Brillouin zone for geometric optimization. The simulation was run with a cutoff energy of 500 eV throughout the computations. These settings ensure the convergence of the total energies to within 1 meV per atom. Structural relaxation proceeded until all forces on atoms were less than  $1 \text{ meV \AA}^{-1}$  and the total stress tensor was within 0.01 GPa of the target value. The physical adsorption energy of H<sub>2</sub>O molecules on the Si–O and carbon surfaces ( $\Delta E_{\text{adsorption}}$ ) was defined as:

$$\Delta E_{\text{adsorption}} = E_{\text{surf}+\text{H}_2\text{O}} - E_{\text{surf}} - nE_{\text{H}_2\text{O}}$$

where  $E_{\text{surf}+\text{H}_2\text{O}}$ ,  $E_{\text{surf}}$  and  $E_{\text{H}_2\text{O}}$  represent the ground-state energies of the substrate binding with the H<sub>2</sub>O compound, the substrate surface, and the H<sub>2</sub>O molecule, respectively, and  $n=3$ .

**Table S2** DFT-calculated values of the physical adsorption energy of H<sub>2</sub>O for carbon nanotubes, pure carbon fibers, and A-SiO<sub>2</sub>.

---

E(surf+H <sub>2</sub> O)/eV	E(surf)/eV	E(H <sub>2</sub> O)/eV	$\Delta E$ /eV
-----------------------------	------------	------------------------	----------------

---

Pure carbon fiber	-337.81517878	-294.98365295	-14.22259985	-0.16373
Carbon nanotube	-916.37993924	-873.21784199	-14.22259985	-0.16477
A-SiO <sub>2</sub>	-784.52511476	-741.16420671	-14.22259985	-0.69311

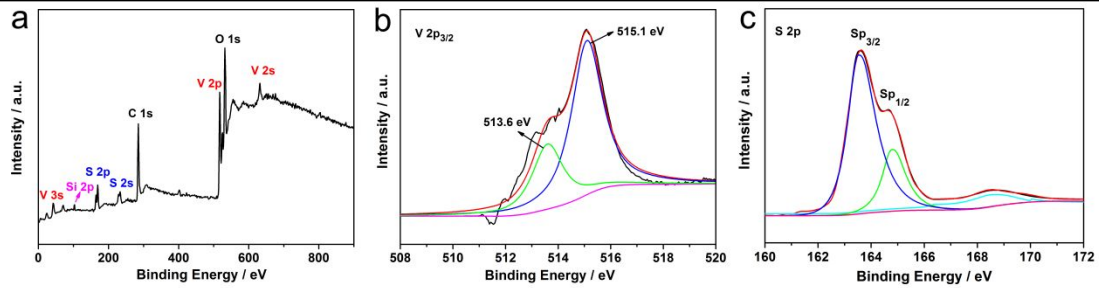


**Figure S7** (a) XPS survey; (b) V 2p<sub>3/2</sub> and (c) S 2p spectrum of the HCC-V<sub>3</sub>S<sub>4</sub> samples.

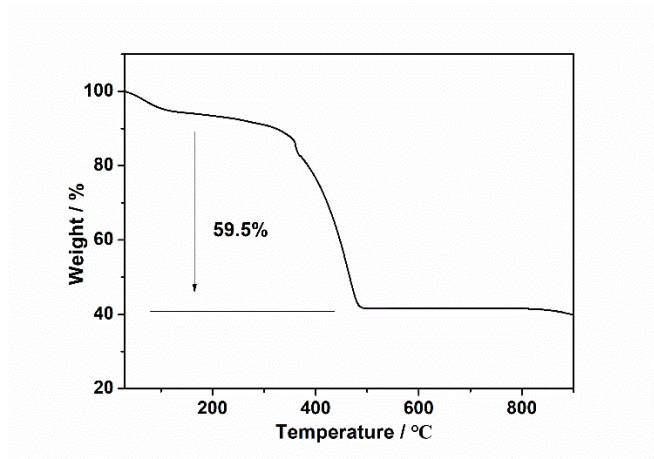


**Figure S8** TGA curve of the HCC-V<sub>3</sub>S<sub>4</sub> in the air atmosphere.

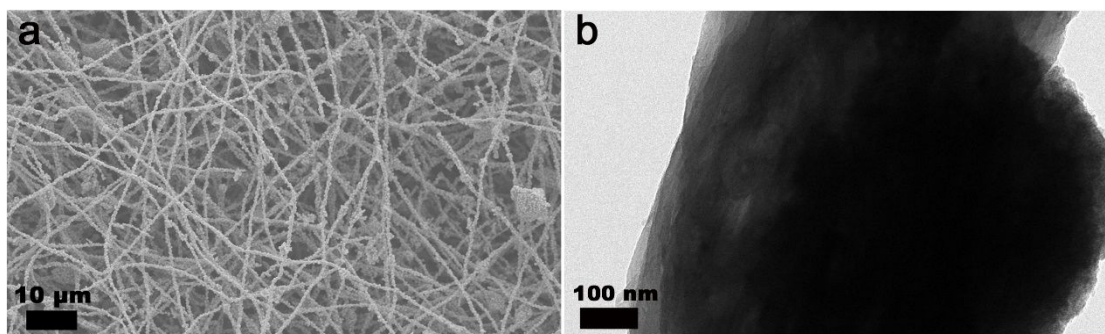


**Figure S9** (a) SEM and (b) TEM images of the HCC- $V_3S_4$  samples.

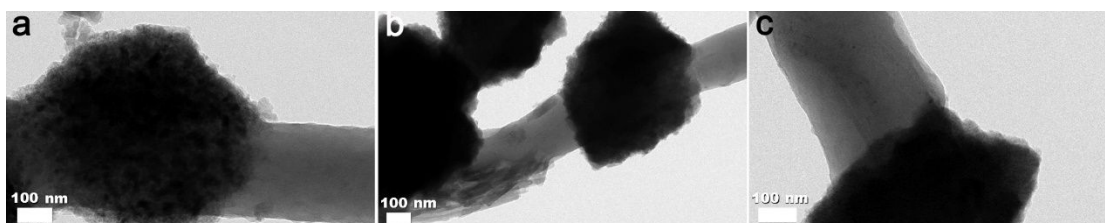


**Figure S10** TEM images of (a) C- $V_3S_4$ , (b) HC- $V_3S_4$ , and (c) CC- $V_3S_4$ .

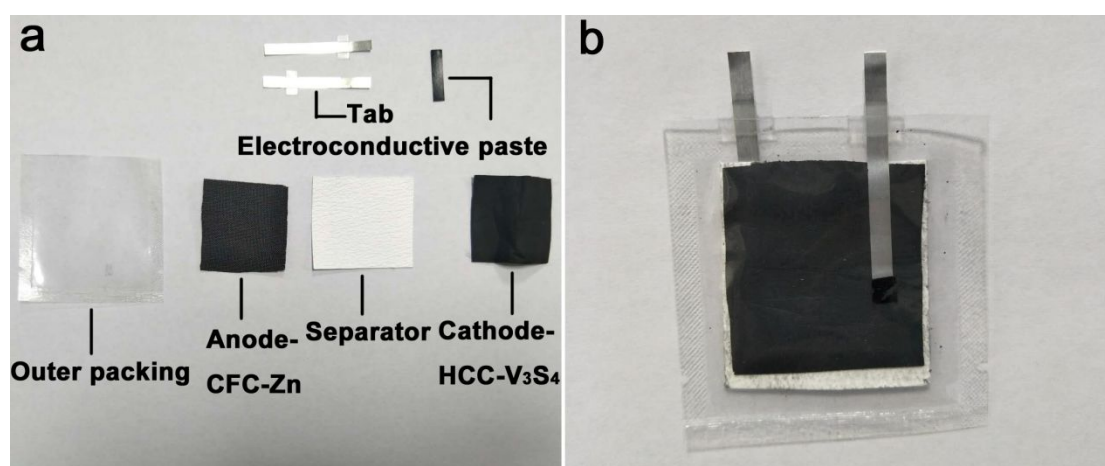


**Figure S11** Macroscopic digital photos of each component for the flexible HCC- $V_3S_4$ /CFC-Zn device.

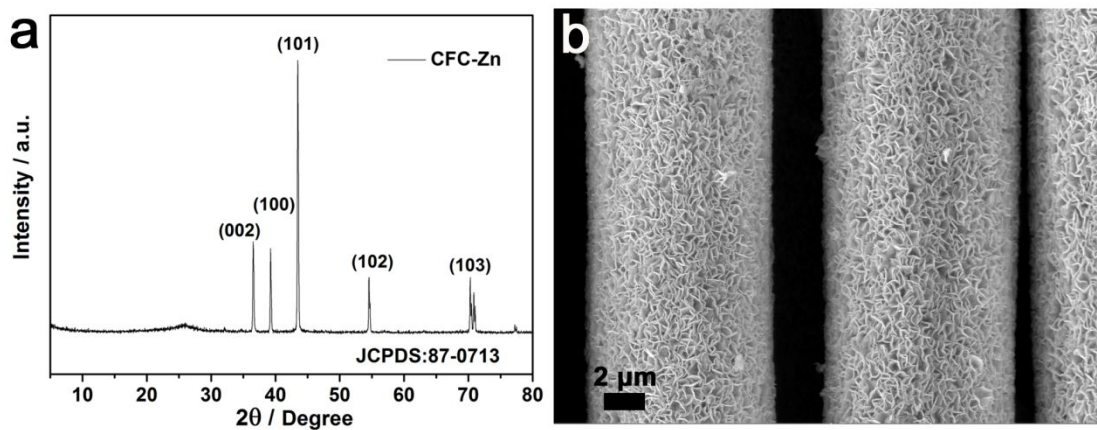


**Figure S12** (a) XRD pattern and (b) SEM image of the CFC-Zn samples.

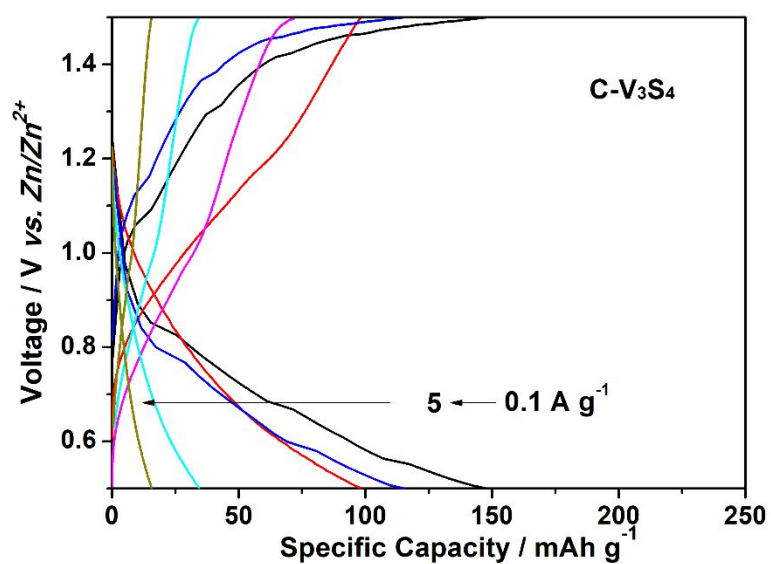


**Figure S13** The selected galvanostatic charge/discharge curves of C-V<sub>3</sub>S<sub>4</sub> at different current densities.

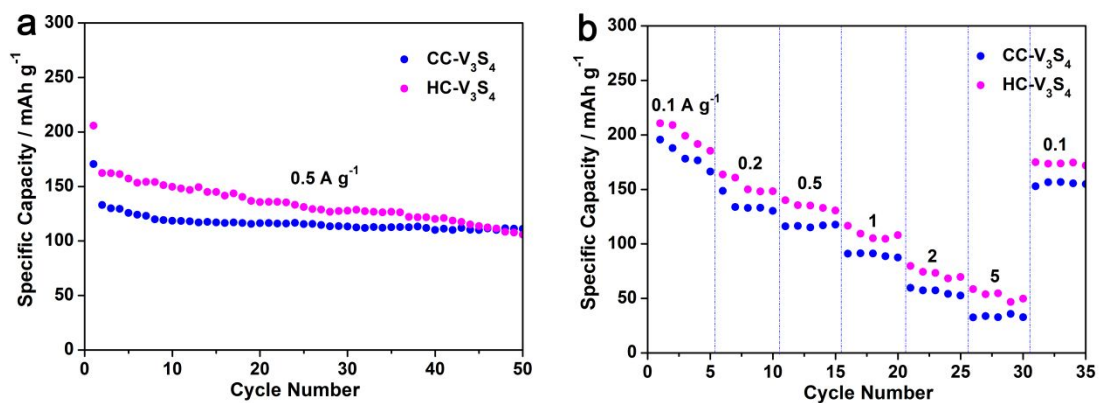


**Figure S14** Electrochemical performance of the flexible systems CC-V<sub>3</sub>S<sub>4</sub>//CFC-Zn and HC-V<sub>3</sub>S<sub>4</sub>//CFC-Zn in the voltage range of 0.5–1.5 V (vs. Zn/Zn<sup>2+</sup>). (a) Cycling performance at 0.5 A g<sup>-1</sup> and (b) rate performance.

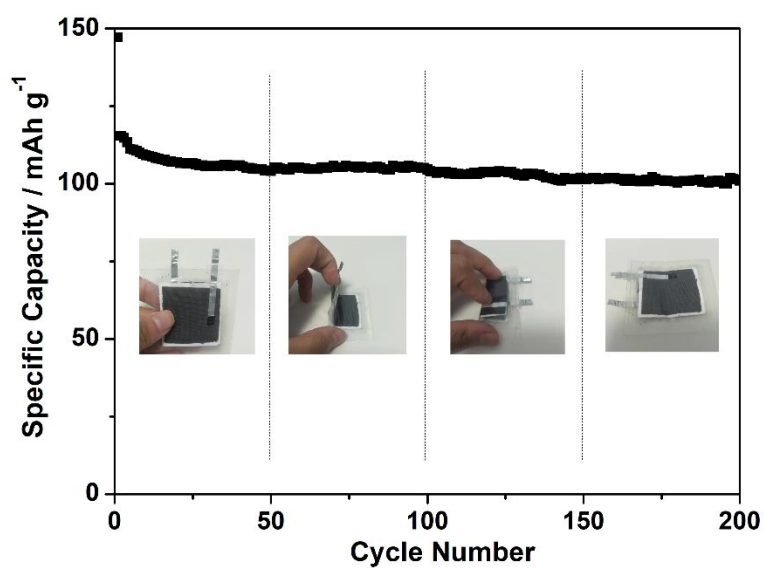


**Figure S15** The flexibility and the corresponding electrochemical performance of the HCC-V<sub>3</sub>S<sub>4</sub>//CFC-Zn device at 2 A g<sup>-1</sup> in the voltage range of 0.5–1.5 V (vs. Zn/Zn<sup>2+</sup>).

**Table S3** A comparison of our work with previously reported electrochemical performance of V-based cathode ZIBs.

Samples	Current density / A g <sup>-1</sup>	Capacity retention / mA h g <sup>-1</sup> (voltage range)	Cycle number	Reference
VS <sub>4</sub> @rGO	1	180 (0.35-1.8 V)	165	[1]
Na <sub>2</sub> V <sub>6</sub> O <sub>16</sub> ·1.63H <sub>2</sub> O nanowire	0.1	231 (0.2-1.6 V)	100	[2]
Na <sub>1.1</sub> V <sub>3</sub> O <sub>7.9</sub> nanoribbons/graphene	0.3	171 (0.4-1.4 V)	100	[3]
Fe <sub>5</sub> V <sub>15</sub> O <sub>39</sub> (OH) <sub>9</sub> ·9H <sub>2</sub> O nanosheet	5	100 (0.4-1.6 V)	300	[4]
VS <sub>2</sub> nanosheet	0.5	111 (0.4-1.0 V)	200	[5]
V <sub>2</sub> O <sub>5</sub> nanosheet	2	113 (0.4-1.4 V)	400	[6]
Na <sub>0.76</sub> V <sub>6</sub> O <sub>15</sub>	0.5	125 (0.4-1.4 V)	100	[7]
<b>This work--- flexible HCC-</b>	0.5	148 (0.5-1.5 V)	200	<b>This work</b>
<b>V<sub>3</sub>S<sub>4</sub>//CFC-Zn</b>	5	102 (0.5-1.5 V)	1000	

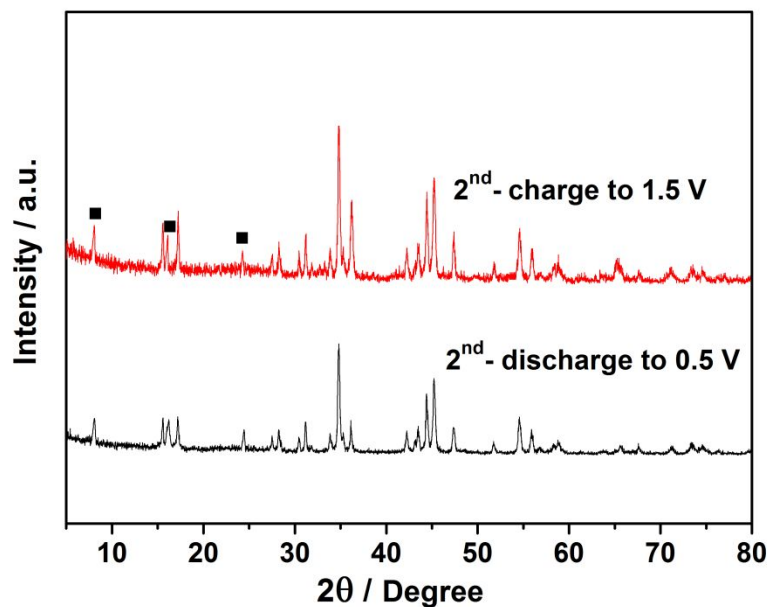


**Figure S16** Ex situ XRD patterns of the HCC- $V_3S_4$  electrodes (a) discharged to 0.5 V at the second cycle and (b) charged to 1.5 V at the second cycle.

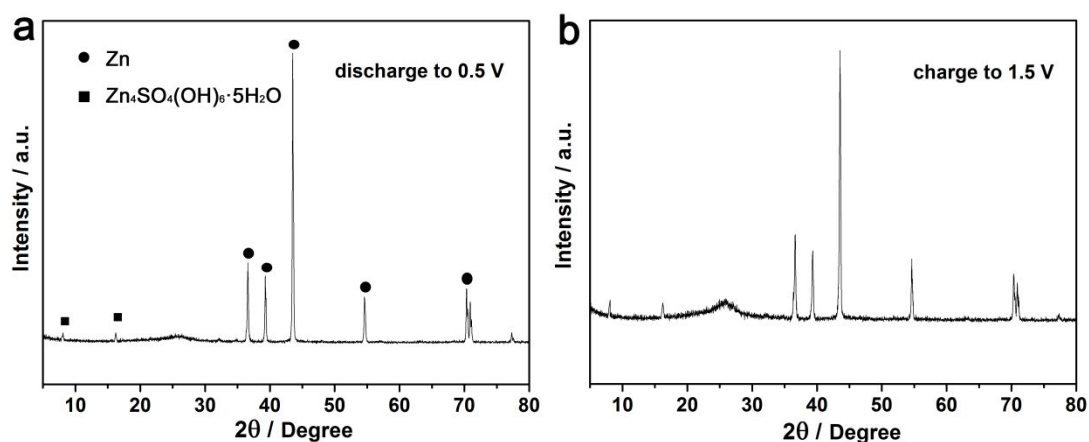


**Figure S17** Ex situ XRD patterns of the HCC-Zn electrodes (a) discharged to 0.5 V at the first cycle and (b) charged to 1.5 V at the first cycle.

**Table S4** WDS composition analysis of the first cycle discharged electrode.

Samples	Composition (at%)					
	V	S	Zn	Si	O	C
1	3.61	4.81	0.88	5.29	10.59	74.82
2	3.73	4.97	0.97	5.03	10.06	75.24
3	3.67	4.89	0.92	5.17	10.34	75.01

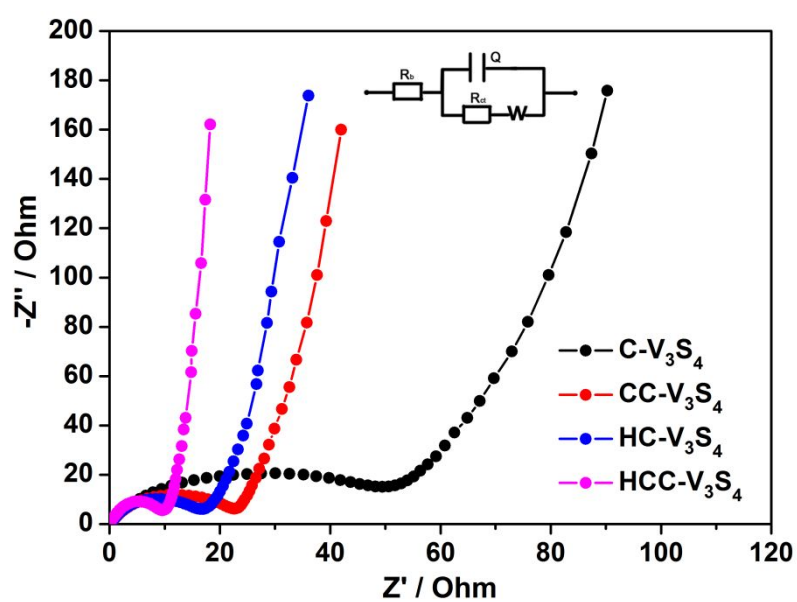


**Figure S18** Electrochemical impedance spectra of the flexible ZIBs employing the HCC-V<sub>3</sub>S<sub>4</sub>, HC-V<sub>3</sub>S<sub>4</sub>, CC-V<sub>3</sub>S<sub>4</sub>, and C-V<sub>3</sub>S<sub>4</sub> as cathodes.

In the Equivalent circuit,  $R_s$  stands for the combination of electrolyte resistance and ohmic resistances of cell components.  $R_{ct}$  is the resistance of the charge transfer resistance of electrochemical reaction.  $Q$ , and  $W$  are the double layer capacitance, and the diffusion controlled Warburg impedance (the value is recorded as  $R_w$ ), respectively. The conductivity of the samples was calculated by the formula:  $\sigma=L/S \cdot R$ , where  $L$  is the thickness of the electrode (80  $\mu\text{m}$ ) and  $S$  is the cross-sectional area of the electrode (4  $\text{cm}^2$ ).  $\sigma_e$  means electron conductivity ( $\sigma_e=L/S \cdot R_{ct}$ ).  $\sigma_i$  is ion conductivity ( $\sigma_i=L/S \cdot R_w$ ). So, the ion and electron values of these different samples were shown in Table S5.

**Table S5** The ion and electron conductivity of that different samples.

Samples	$\sigma_e / \times 10^{-2} \text{ S} \cdot \text{m}^{-1}$	$\sigma_i / \times 10^{-2} \text{ S} \cdot \text{m}^{-1}$
HCC- $\text{V}_3\text{S}_4$	2.05	3.91
HC- $\text{V}_3\text{S}_4$	1.10	0.86
CC- $\text{V}_3\text{S}_4$	0.89	0.66
C- $\text{V}_3\text{S}_4$	0.41	0.07

## References

- (1) Qin, H.; Yang, Z.; Chen, L.; Chen, X.; Wang, L. A High-rate Aqueous Rechargeable Zinc Ion Battery Based on the  $\text{VS}_4@\text{rGO}$  Nanocomposite. *J. Mater. Chem. A* **2018**, *6* (46), 23757-23765.
- (2) Hu, P.; Zhu, T.; Wang, X.; Wei, X.; Yan, M.; Li, J.; Luo, W.; Yang, W.; Zhang, W.; Zhou, L.; Zhou, Z.; Mai, L. Highly Durable  $\text{Na}_2\text{V}_6\text{O}_{16} \cdot 1.63\text{H}_2\text{O}$  Nanowire Cathode for Aqueous Zinc-Ion Battery. *Nano Lett.* **2018**, *18* (3), 1758-1763.
- (3) Cai, Y.; Liu, F.; Luo, Z.; Fang, G.; Zhou, J.; Pan, A.; Liang, S. Pilotaxitic

$\text{Na}_{1.1}\text{V}_3\text{O}_{7.9}$  Nanoribbons/graphene as High-performance Sodium Ion Battery and Aqueous Zinc Ion Battery Cathode. *Energy Storage Mater.* **2018**, *13*, 168-174.

(4) Peng, Z.; Wei, Q.; Tan, S.; He, P.; Luo, W.; An, Q.; Mai, L. Novel Layered Iron Vanadate Cathode for High-capacity Aqueous Rechargeable Zinc Batteries. *Chem. Commun. (Camb)* **2018**, *54* (32), 4041-4044.

(5) He, P.; Yan, M.; Zhang, G.; Sun, R.; Chen, L.; An, Q.; Mai, L. Layered  $\text{VS}_2$  Nanosheet-Based Aqueous Zn Ion Battery Cathode. *Adv. Energy Mater.* **2017**, *7* (11), 1601920.

(6) Zhou, J.; Shan, L.; Wu, Z.; Guo, X.; Fang, G.; Liang, S. Investigation of  $\text{V}_2\text{O}_5$  as A Low-cost Rechargeable Aqueous Zinc Ion Battery Cathode. *Chem. Commun. (Camb)* **2018**, *54* (35), 4457-4460.

(7) Guo, X.; Fang, G.; Zhang, W.; Zhou, J.; Shan, L.; Wang, L.; Wang, C.; Lin, T.; Tang, Y.; Liang, S. Mechanistic Insights of  $\text{Zn}^{2+}$  Storage in Sodium Vanadates. *Adv. Energy Mater.* **2018**, *8* (27), 1801819.